Published in final edited form as:
Ultrasound Med Biol. 2012 November ; 38(11): 1989–1997. doi:10.1016/j.ultrasmedbio.2012.07.019.

ACOUSTIC RADIATION FORCE FOR VASCULAR CELL THERAPY: *IN VITRO* VALIDATION

Mehmet Kaya, **Catalin Toma**, **Jianjun Wang**, **Michelle Grata**, **Huili Fu**, **Flordeliza S. Villanueva**, and **Xucai Chen**
Center for Ultrasound Molecular Imaging and Therapeutics, Heart and Vascular Institute, University of Pittsburgh Medical Center, Pittsburgh, PA

Abstract

Cell-based therapeutic approaches are attractive for the restoration of the protective endothelial layer in arteries affected by atherosclerosis or following angioplasty and stenting. We have recently demonstrated a novel technique for the delivery of mesenchymal stem cells (MSCs) that are surface-coated with cationic lipid microbubbles (MBs) and displaced by acoustic radiation force (ARF) to a site of arterial injury. The objective of this study was to characterize ultrasound parameters for effective acoustic-based delivery of cell therapy. *In vitro* experiments were performed in a vascular flow phantom where MB-tagged MSCs were delivered towards the phantom wall using ARF generated with an intravascular ultrasound catheter. The translation motion velocity and adhesion of the MB-cell complexes were analyzed. Experimental data indicated that MSC radial velocity and adhesion to the vessel phantom increased with the time-averaged ultrasound intensity up to 1.65 W/cm^2, after which no further significant adhesion was observed. Temperature increase from baseline near the catheter was 5.5 ±0.8°C with this setting. Using higher time-averaged ultrasound intensities may not significantly benefit the adhesion of MB-cell complexes to the target vessel wall (p=NS), but could cause undesirable biological effects such as heating to the MB-cell complexes and surrounding tissue. For the highest time-averaged ultrasound intensity of 6.60 W/cm^2, the temperature increase was 11.6 ±1.3°C.

Keywords

Ultrasound; Microbubble; Mesenchymal stem cell; Acoustic radiation force; Intravascular catheter

INTRODUCTION

Ultrasound microbubble (MB) contrast agents have been widely used for numerous applications including enhancement of the blood pool for improved endocardial definition on echocardiographic imaging and gene and drug delivery (Unger et al. 2003; Klibanov 2002; Ferrara et al. 2007; Villanueva 2008; Hitchcock and Holland 2010, Qin et al 2009). It has been shown that it is possible to change the flow patterns of microbubbles if the ultrasound imaging parameters create significant acoustic radiation force (ARF) (Dayton et

Corresponding author: Dr. Flordeliza S. Villanueva, Center for Ultrasound Molecular Imaging and Therapeutics, Heart and Vascular Institute, 200 Lothrop Street, A351 PUH, Pittsburgh, PA 15213, Phone: 412-647-5840, Fax: 412-647-4227, villanuevafs@upmc.edu, Website: www.imagingtherapeutics.pitt.edu.

al. 1999; Zhao et al. 2004). Thus, microbubbles and their therapeutic payload can potentially be directed towards a specific target using ultrasound. ARF was first described by King (King 1934) and potential applications of this phenomenon have been suggested. Primary radiation force arises from the phase difference between the driving acoustic pressure and the oscillation of a particle or microbubble in a continuous medium. For axi-symmetric objects like MBs in a plane traveling wave field, the primary ARF is in the direction of sound propagation. The effects of ARF on bubbles in general (Crum 1975, Lee and Wang 1993, and Leighton 1994) and on contrast agents in particular (Dayton 1997, 1999, 2002), have been previously described and form the basis for the study described in this report.

Endothelial progenitor cells (EPCs) and mesenchymal stem cells (MSCs) may participate in effective restoration of functional endothelium following vascular injury (Yue et al. 2008; Forte et al. 2008). However, intra-arterially delivered cells would have to overcome significant hydrodynamic forces to adhere under flow, which is why experimental *in vivo* delivery of EPCs or MSCs to a specific vascular segment usually requires prolonged cessation of flow to that segment, an ineffective and impractical option from a clinical standpoint. We have previously reported a novel *in vivo* method for effective targeted delivery of stem cells to a site of arterial injury using ARF (Toma et al. 2011). By tagging MSCs with gas-filled lipid MBs, the MB-cell complexes were selectively pushed with acoustic energy to the endoluminal surface of the arterial wall.

Previous work demonstrated the use of targeted microbubbles for drug and gene delivery enhanced by ultrasound radiation force both *in vivo* and *in vitro*. In one of those earlier studies, Rychak et al. (2005) showed that acoustic pressure mechanism was suitable for achieving targeted microbubble delivery in high-flow vessels and quantified the dependence of microbubble adhesion on acoustic pressure and shear rate *in vitro*. Hallow et al (2007) evaluated the intracellular uptake and cell death when microbubbles and a drug were targeted into vascular endothelial cells (ECs) and smooth muscle cells (SMCs) in the coronary artery using ARF. They concluded that significant intracellular uptake of molecules can be targeted into ECs and SMCs by ultrasound-enhanced delivery. Phillips et al. (2008) suggested that intravascular ultrasound (IVUS) is essential to enhance gene transfection from microbubble carriers to the vessel wall *in vivo* (Phillips et al. 2008). Their group demonstrated that IVUS catheter mediated plasmid DNA transfection from microbubble carriers to the porcine coronary artery wall following balloon angioplasty. Patil et al. (2009) proposed an approach for simultaneously pushing and imaging microbubbles in a real-time environment. They concluded that for blood vessels of large size, and flow velocities in a certain range, radiation force generated using customized dual frequency sequences was able to translate microbubbles across the vessel resulting in accumulation of the microbubbles at the targeted wall. Another study by Gessner et al. (2009) presented a description of a prototype dual-frequency transducer which enabled simultaneous high-resolution imaging with the application of radiation force to enhance targeting and adhesion *in vitro* and *in vivo*. They observed a 7 fold increase in image signal intensity after radiation force enhanced targeting compared to standard rheologically-mediated targeting. Ultrasound based molecular imaging has also been used to image vascular pathology and to guide localized drug delivery in blood vessels (Patil et al. 2011).

Our study differs from previous drug and gene delivery techniques in that we attached the MBs on the surface of vascular cells such as stem cells to form MB-cell complexes before injection and the ARF on these complexes provided a means of delivering the cells to the treatment site. Therefore, the MBs themselves are not targeted, but they serve as carriers for MSCs. We have demonstrated previously that the MSCs could be successfully delivered to the endothelium in the abdominal aorta through *in vivo* experiments in a rabbit model (Toma et al, 2011).

To foster clinical translation of this novel cell delivery strategy, the objective of the current study was to further analyze and optimize ultrasound parameters for the delivery of biological cells such as stem cells using an *in vitro* flow model. We investigated how increasing the time-averaged ultrasound intensity delivered to the microbubbles through manipulation of acoustic pressure and duty cycle would modulate the extent of cell adhesion. We also explored whether there was an optimal combination of ultrasound parameters for this ultrasound and flow system that were sufficient to successfully push the majority of MB-labeled cells to the phantom wall. It is essential to define optimal ultrasound parameters since simply increasing time-averaged ultrasound intensities may not substantially improve adhesion of MB-cell complexes to the target vessel wall, but could cause undesirable biological effects such as heating to the MB-cell complexes and surrounding tissue.

The ARF on the MB can be calculated once the dynamic behavior of the bubble is determined. The short-term time-averaged force over one acoustic cycle can be expressed as: $\langle F_R \rangle = E_0(\pi R_0^2)Y_p$ where $E_0 = \frac{p_A^2}{2\rho_l c_l^2}$ is the energy density of the acoustic wave and the radiation force function is given by $Y_p = \frac{4c_l}{\omega_0 R_0} \frac{\delta_{tot}}{[1-(\omega/\omega_0)^2]^2 + \delta_{tot}^2(\omega/\omega_0)^2}$. This formulation can be considered as an alternative form of the equation (4.136) in Leighton (1994). Due to the presence of radiation force, the microbubble will experience translational motion (Crum 1975; and Watanabe and Kukita 1993). We are interested in the translational motion of a MB-cell complex when the ARF is used to delivery vascular cells for therapeutic purposes. Due to the much larger size of MSC compared with the MB used, the attainable translational velocity of the MB-cell complex is much smaller when compared with a single MB in the same ultrasound field. The ARF on the MSC can be obtained as a limiting case of the general theory presented by Chen and Apfel (1996). The force is in the direction of acoustic wave propagation and can be expressed as: $\langle F_R \rangle_c = E_0(\pi R_c^2)Y_p$ where R_c is Y_p radius of the cell, and is the radiation force function. For the frequency range of relevance, the stem cell can be considered as a Rayleigh scatter, and the radiation force function reduces to: $Y_p = 4[(\gamma_k/3 - \gamma_\rho/9)^2 + 2(\gamma_\rho/9)^2](k_l R_c)^4$ where $\gamma_\rho = 3(\rho_c - \rho_l)/(2\rho_c + \rho_l)$ is the density contrast between the cell and the host medium, and $\gamma_k = (\kappa_c - \kappa_l)/\kappa_l = (\rho_l c_l^2)/\rho_c c_c^2 - 1$ is the compressibility contrast between the cell and the host medium. For a stem cell with 10 μm radius driven at a 1.7 MHz and 100 kPa of acoustic pressure amplitude, and using the mechanical properties of 0.9% saline as the surrounding medium, the ARF is calculated to be 5.3×10^{-16} *N*, six orders of magnitude smaller than the ARF on a bubble of concern. Therefore, the ARF on the cell can be ignored when the translational motion of the MB-cell complex is evaluated. Once the ARF on the bubble is determined, either analytically or numerically, the translational motion of the MB-cell complex can be estimated. Strictly speaking, a coupled equation for the radial and translational motion of the MB needs to be considered. This treatment is outside the scope of work presented here.

METHODS

Experimental design and setup

The studies of radiation force *in vitro* were performed in a flow phantom that allowed simultaneous optical and acoustical observation of MB-cell complexes. The schematic of the experimental setup is illustrated in Figure 1. The phantom vessel was made of polyvinyl chloride (PVC) tubing with an internal diameter of 3.5 mm. The suspension of MB-cell complexes was prepared in a reservoir and withdrawn through the phantom vessel by a precision syringe pump (PHD 2000, Harvard Apparatus) with a 60 ml syringe (Becton

Dickinson). A flow rate of 40 ml/min was chosen such that the wall shear stress (1.1 Pa) approximated that of average coronary blood flow (Doriot et al. 2000).

An intravascular ultrasound catheter with a 2-mm long 1.7 MHz transducer (MicroSonic SV, Ekos Corp) was placed along the center of the phantom. The ultrasound catheter was driven by a power amplifier (Model 100A250A, Amplifier Research) coupled to an arbitrary waveform generator (Model 33250A, Agilent). A calibrated hydrophone (HGL-0200, Onda Corp) was used for calibration of the acoustic system. The phantom vessel was placed under an Olympus IX81 inverted fluorescence microscope (Olympus Corp) equipped with a high sensitivity EMCCD camera (C9100-2, Hamamatsu Photonics K.K.). Digital fluorescence movies of MB-labeled fluorescent MSCs (MB-cell complexes, or MB-MSC complexes in this study) flowing through the phantom were captured at a frame rate of 50 frames/second. The optical focus of the microscope was co-localized with the ultrasound focus for continuous optical observation and recording. A long working distance low magnification Olympus 4x objective was used for visualization of the flow phantom, with a field of view of 2 mm × 2 mm, sufficient to cover one side of the flow phantom from the catheter to the vessel wall.

Fluorescent labeled MB-cell complexes were advanced through the vessel phantom while being visualized and continuously recorded for a total of 20 seconds: 5 seconds before ultrasound was turned on, followed by 10 seconds of ultrasound exposure, and another 5 seconds after ultrasound was turned off. After each experiment, the flow phantom was flushed with phosphate buffered saline (PBS) to remove all the adhered MB-cell complexes from the targeted focal area. Control experiments were performed with MSCs with no MBs.

Microbubble formulation

Cationic lipid MBs were made from a mixture of lipids 1,2-distearoyl-sn-glycero-3-phosphocholine (DSPC) and 1,2-distearoyl-sn-glycero-3-ethylphosphocholine (DSEPC) (Avanti Polar Lipids) and polyethylene glycerol stearate (Sigma-Aldrich). The DSEPC carries the quaternary ammonium ion, giving the bubble a cationic charge. The mixture dissolved in chloroform was evaporated with a steady Argon gas stream and degassed overnight under house vacuum. The dried lipids mixture was re-hydrolyzed in sterile saline and sonicated in the presence of perfluorocarbon gas. The MB suspension was then washed 3 times with sterile saline to eliminate unbound lipids and smaller microbubbles to reach a desired size distribution. The size distribution of the cationic lipid microbubbles was analyzed using a Multisizer 3 Coulter Counter (Beckman Coulter Inc.) and the charge on the microbubbles was quantified using a Zetasizer Nano-Zs90 (Malvern Instruments).

Cell culture

Low passage human MSCs (Lonza) were expanded in 10% hMSC culture media (Lonza). Prior to use, the cells were fluorescently labeled with 0.5 μM cytoplasmic dye (CellTracker Green, CMFDA, Invitrogen) for 30–60 minutes. The cells were then trypsinized using 1:4 dilution of trypsin–versene (Part 17–161, Lonza) mixture in PBS and washed in PBS.

The viscosity of the buffer solution for MB-MSCs was adjusted to that of blood at body temperature (4×10^{-3} Pa·s) using polyvinylpyrrolidone (PVP) (Sigma-Aldrich). The kinematic viscosity measurements of the solution were performed using a U-tube, glass capillary viscometer (Rheotek Inc.).

MSCs were mixed for 5 minutes with cationic MBs at a ratio of 1:40, previously experimentally shown by us to be optimal for achieving ARF-induced MB-MSC adhesion to a vascular surface (Toma et al. 2011). The MB-MSC suspension was then diluted to a concentration of 5×10^3 cells/ml in a sample reservoir, with a solution of PVP and PBS

adjusted to include 1 mM of calcium chloride ($CaCl_2$) and 0.5 mM of magnesium chloride (MgCl).

Flow cytometry

Flow cytometry was performed to quantify MB-MSC association (FACSCalibur, Becton Dickinson), based on the observation that MB attachment to the MSC surfaces increases their side scatter (SSC) due to the multiple reflective surfaces of the MBs present on the cells as described previously (Toma et al. 2011). Before each experiment, the presence of microbubbles on the surface of the MSCs was verified with flow cytometry and microscopy.

Image analysis

Digitally recorded fluorescence images and videos were transferred to ImageJ (Rasband 1997–2011) for further analysis. An algorithm was incorporated into the software to produce maximum intensity persistence of the MB-MSC images. Particle trajectory, radial velocity (u_r), and amount of cell adhesion were measured. The radial velocity of the MB-cell complexes, which represents the translational motion conferred by ARF on the MB-cell complexes, was calculated by measuring the radial displacement in a known number of frames and the time elapsed to travel that distance. The number of cells adhering or intermittently adherent to the wall during 10 seconds of ultrasound exposure, as well as the number of cells persistently adherent 5 seconds after the ultrasound was turned off were counted by visually tracking and analyzing the images.

Protocol

A total of 18 samples were used to measure the radial velocities of the MB-cell complexes. We investigated the effect of the following parameters on the radial velocity and adhesion of the MB-cell complexes: acoustic pressure (100 kPa, 250 kPa, 500 kPa, 750 kPa and 1 MPa), duty cycle (DC) (10%, 20% and 60%), pulse length (5 cycles, 10 cycles and 20 cycles) and corresponding pulse intervals (Table 1). Particle radial velocities derived from the experimental data and model predictions were compared. The axial velocities of the MB-cell complexes (in the direction of the fluid flow) were measured in the absence of ultrasound exposure.

Temperature measurements

We performed temperature measurements to determine heating effects at higher time-averaged ultrasound intensities. A thermocouple connected to a multimeter (114 True RMS Digital Multimeter, Fluke Corp.) was placed in the immediate vicinity of the ultrasound catheter tip within the phantom vessel under static physiological flow conditions (40 ml/min). The temperature increase from baseline temperature (approximately 22°C) was measured.

Statistics

The experimental data was expressed as mean ± standard error of the mean. Experimental groups were compared using an analysis of variance on data by the Single Factor ANOVA model. Statistical significance was defined as p-values < 0.05.

RESULTS

MSC association with cationic MBs

The mean diameter of the MBs s was 2.54±0.91 μm and mean electrostatic charge was 51±9 mV. In addition to microscopic examination, flow cytometry verified the association of MBs with the negatively charged MSCs (Figure 2). MB attachment to the cell led to a significant

increase in the amount of orthogonal scattered light (side-scatter) in comparison with MSCs alone to in flow cytometry.

Axial velocity (u_z)

Theoretically, the main flow pattern in the phantom is concentric flow. The experimental values for axial velocity were similar to the theoretical values. The maximum axial velocity (10.9±0.7 cm/s) occurred at 0.78 mm from the transducer tip and the minimum velocities were measured near the transducer tip and close to the vessel wall (Figure 3).

Radial velocity of the MB-cell complex (u_r)

The experimentally measured radial velocity of the MB-cell complexes u_r for various combinations of ultrasound parameters (n=3 experiments per condition) are shown in Figure 4, which groups the data by the time-averaged ultrasound intensity for a given combination of acoustic pressure and number of cycles (5, 10, or 20) per pulse. The time-averaged ultrasound intensity was the major determinant of the MB-MSC radial velocity, independent of the duty cycle/pulse length configurations (5 cycles, 10 cycles and 20 cycles and corresponding pulse intervals) (p=NS for multiple comparisons within the group with same acoustic pressure and duty cycles). This was further evidenced by comparing the second group (with 102 kPa and 60% DC) and third group (with 250 kPa and 10% DC) of parameters, both producing the same time-averaged ultrasound intensity of 0.21 W/cm^2 and resulting in similar MB-MSC radial velocities (1.9±0.2 cm/s and 2.0±0.3 cm/s respectively, p=NS).

In Figure 5, the mean radial velocity of the MB-cell complexes for each of the time averaged ultrasound intensities represented in Figure 4 was plotted against the time-averaged ultrasound intensity. u_r was nearly proportional to the time-averaged ultrasound intensity up to 0.83 W/cm^2. The maximum u_r of 6.6±0.4 cm/s was obtained with a time-averaged ultrasound intensity of 1.65 W/cm^2. Note that this was near the velocity limit that the camera system could report at the achievable frame rate with the phantom used.

In the control group, MSCs with no MB association were not pushed in the radial direction.

Adhesion

The total numbers of MB-MSCs adhered on the vessel wall during 10 seconds of ultrasound exposure and 5 seconds after the ultrasound was turned off are shown in Figure 6. Following ultrasound mediated MSC displacement and adhesion to the wall (solid line), some of the adherent complexes were displaced downstream after ultrasound was turned off due to unopposed shear stress (dashed line). The number of persistently adherent MSCs increased with the time-averaged ultrasound intensity (dashed line), up to a time-averaged ultrasound intensity of 1.65 W/cm^2 (Fig. 5), corresponding to the highest radial velocity measured. No appreciable increase in adhesion was observed with higher time-averaged ultrasound intensity under the flow conditions tested.

No adhesion was observed on the vessel wall for the control group, in which no MBs were attached to MSCs.

Trajectory

For a given MB-cell complex originating at a specific point within the vessel, its flow trajectory can be plotted as the net vector resulting from the measured radial velocity and theoretical axial flow profile at various ultrasound parameter combinations (Figure 7). For simplicity, only MB-cell complexes entering the field of view at 3 different locations (1.35 mm, 1 mm, and 0.6 mm away from the vessel wall) were plotted. For those complexes

entering the ultrasound field near the center of the flow phantom (1.35 mm from the vessel wall or 0.4 mm from the center of the transducer), all reached the vessel wall with 500 kPa and 20% DC (1.65 W/cm^2) or higher equivalent time-averaged intensity) but failed to reach the wall with other ultrasound parameter combinations. For those complexes entering the ultrasound field closer to the vessel wall (0.6 mm), all of the MB-cell complexes reached the wall at or above an acoustic pressure of 250 kPa and 10% DC (0.21 W/cm^2).

Overall, all the MB-cell complexes entering the US field were expected to be delivered to the vessel wall with a time-averaged intensity of 1.65 W/cm^2 or higher for the volume flow rate used. This intensity level depends on the axial flow velocity (governed by the volume flow rate) and the length of the vessel included within the ultrasound field.

The actual flow trajectories of the MB-cell complexes are shown in Figure 8 as images after processing for maximum intensity persistence, for various time-averaged ultrasound intensities.

Temperature measurements

At the physiological flow conditions (40 ml/min) the temperature near the tip of the ultrasound catheter increased 1.3±0.3°C for the time-averaged ultrasound intensity of 0.83 W/cm^2 and 5.5 ±0.8°C for the time-averaged ultrasound intensity of 1.65 W/cm^2. For the higher time-averaged ultrasound intensities of 4.13 and 6.60 W/cm^2, the temperature increase from the baseline was recorded as 8.7 ±0.9°C and 11.6 ±1.3°C respectively.

CONCLUSIONS AND DISCUSSION

Our group was the first to demonstrate the concept that therapeutic vascular cells can be delivered *in vivo* using ARF (Toma et al. 2011). In our prior work, we attached cationic uMBs to MSCs via electrostatic interaction, and found that ARF caused not only acute attachment of MSCs to injured rabbit aortic segments *in vivo*, but that the cells persisted and engrafted over time. In the particular scenario of endoluminal cell delivery for arterial repair, this technology appears to be more efficient compared with other techniques using EPCs loaded with supermagnetic iron oxide nanoparticles in arteries of similar caliber, which resulted in about 25 times less adhesion to the vessel wall (Kyrtatos et al. 2009; Pislaru et al. 2006).

In order to optimize this novel approach at directing the translation motion of MB-MSCs using ARF, we performed *in vitro* testing to optimize the ultrasound delivery parameters. Experimental data demonstrated that the time-averaged ultrasound intensity is the main determinant of the radial translational velocity and adhesion to the vessel wall. This indicates that we could use lower acoustic pressure with higher duty cycles to achieve similar translational motion of the MB-cell complex. Theoretically this pulse sequence could be less destructive to MB.

Experimental data indicated that the number of MSCs adhering to the wall increased with the radial velocity of the MB-cell complexes, as more and more complexes were able to reach the vessel wall during the finite time when the MB-cell complexes were within the finite size of the ultrasound field. Increasing the time-averaged ultrasound intensity further beyond an ultrasound intensity of 1.65 W/cm^2 did not increase the extent of adhesion of MB-cell complexes to the wall, for the flow condition used. This is to be expected, however, as all of the MB-cell complexes reached the vessel wall due to the ARF for any time-averaged ultrasound intensity above 1.65 W/cm^2. Therefore, a time-averaged intensity higher than this value should not be used, considering heating and other potential ultrasound related concerns such as bubble destruction at higher ultrasound intensities.

The conjugation of the MBs with the MSCs is essential to the success of ARF for vascular stem cell therapy. The ARF on the MSC alone is six orders of magnitude smaller than that on the MBs for identical ultrasound conditions. No significant influence on MSC trajectory nor adhesion was observed when no MBs were attached to the MSC surface.

Study limitations

One limitation of this study was the capability of the optical imaging system. It was not possible to measure the radial velocity higher than 6.8 cm/s as the MB-MSC would have traversed the region of interest in less than one frame. However, we could still quantify the amount of adhesion on the phantom vessel wall for all acoustic parameters considered. Another limitation is possible measurement error due to the cylindrical shape of the phantom vessel wall and difficulty in focusing consistently at the same region of interest.

Significance of the study

In spite of these limitations, the *in vitro* analysis presented here identifies an optimal set of acoustic parameters for the ultrasound and flow system that has a potential for vascular cell-based therapies. Therapeutics based on progenitor cells can be potentially applied to a variety of applications, such as endothelial regeneration following angioplasty, increasing the patency of saphenous vein grafts used in coronary artery by-pass surgery, or the treatment of focal large vessel vasculidities. Optimization of the acoustic based cell delivery is a key element in progressing towards a cell delivery method that does not entail flow cessation, thus making it clinically attractive. While we only presented results with MSC, other cell types can be delivered for various disease models using similar technique developed in our study.

Acknowledgments

We would like to thank Frances Lutka and Emily Etling for their help with cell preparation and Dr. Marina Kameneva for her help with viscosity measurements. This work was funded by the Center for Ultrasound Molecular Imaging and Therapeutics at the University of Pittsburgh Medical Center. Drs. Kaya, Chen, Wang, Fu, Villanueva, and Toma were funded in part by DPI ODO003819, 5RC1EB010533, or R21HL102531 from the National Institutes of Health.

References

Bechmann M, Thiel MJ, Neubauer AS, Ullrich S, Ludwig K, Kenyon KR, Ulbig MW. Central corneal thickness measurement with a retinal optical coherence tomography device versus standard ultrasonic pachymetry. Cornea. 2001; 20:50–54. [PubMed: 11189004]

Behrendt D, Ganz P. Endothelial function: From vascular biology to clinical applications. Am J Cardiol. 2002; 90(10C):40L–48L.

Chen X, Apfel RE. Radiation force on a spherical object in an axisymmetric wave field and its application to the calibration of high-frequency transducers. J Acoust Soc Am. 1996; 99(2):713–724. [PubMed: 8609305]

Crum L. Bjerknes forces on bubbles in a stationary sound field. J Acoust Soc Am. 1975; 57:1363–1370.

Dayton PA, Morgan KE, Klibanov A, Brandenburger G, Nightingale K, Ferrara KW. A preliminary evaluation of the effects of primary and secondary radiation forces on acoustic contrast agents. IEEE Trans Ultrason Ferroelec Freq Contr. 1997; 44:1264–1277.

Dayton PA, Klibanov A, Brandenburger G, Ferrara K. Acoustic radiation force *in vivo*: a mechanism to assist targeting of microbubbles. Ultrasound in Medicine and Biology. 1999; 25(8):1195–1201. [PubMed: 10576262]

Dayton PA, Allen JS, Ferrara KW. The magnitude of radiation force on ultrasound contrast agents. J Acoust Soc Am. 2002; 112:2183–2192. [PubMed: 12430830]

Devin C. Survey of thermal, radiation, and viscous damping of pulsating air bubbles in water. J Acoust Soc Am. 1959; 31:1654–1667.

Doriot PA, Dorsaz PA, Dorsaz L, De Benedetti E, Chatelain P, Delafontaine P. In-vivo measurements of wall shear stress in human coronary arteries. Coron Artery Dis. 2000; 11:495–502. [PubMed: 10966136]

Ferrara KW, Pollard RE, Borden MA. Ultrasound microbubble contrast agents: fundamentals and application to drug and gene delivery. Annual Rev Biomed Eng. 2007; 9:415–47. [PubMed: 17651012]

Forte A, Finicelli M, Mattia M, Berrino L, Rossi F, De Feo M, Cotrufo M, Cipollaro M, Cascino A, Galderisi U. Mesenchymal stem cells effectively reduce surgically induced stenosis in rat carotids. J Cell Physiol. 2008; 217(3):789–99. [PubMed: 18690654]

Gessner, R.; Lukacs, M.; Lee, M.; Tsuruta, J.; Foster, FS.; Dayton, PA. Radiation force-enhanced targeted imaging and near real-time molecular imaging using a dual-frequency high-resolution transducer: In-vitro and in-vivo results. IEEE International Ultrasonics Symposium Proceedings; 2009; 2009. p. 9-12.

Hallow DM, Mahajan AD, Prausnitz MR. Ultrasonically targeted delivery into endothelial and smooth muscle cells in ex vivo arteries. J Control Release. 2007 Apr; 118(3):285–293. [PubMed: 17291619]

Hitchcock KE, Holland CK. Ultrasound-assisted thrombolysis for stroke therapy: better thrombus break-up with bubbles. Stroke. 2010 Oct; 41(10 Suppl):S50–3. [PubMed: 20876505]

King LV. On the acoustic radiation pressure on spheres. Proc R Soc London. 1934; A 147:212–240.

Klibanov AL. Microbubble contrast agents - Targeted ultrasound imaging and ultrasound-assisted drug-delivery applications. Investigative Radiology. 2006; 41(3):354–62. [PubMed: 16481920]

Kyrtatos PG, Lehtolainen P, Junemann-Ramirez M, Garcia-Prieto A, Price AN, Martin JF, Gadian DG, Pankhurst QA, Lythgoe MF. Magnetic tagging increases delivery of circulating progenitors in vascular injury. JACC Cardiovasc Interv. 2009 Aug; 2(8):794–802. [PubMed: 19695550]

Lee CP, Wang TW. Acoustic radiation force on a bubble. J Acoust Soc Am. 1993; 93(3):1637–1640.

Leighton, TG. The Acoustic Bubble. San Diego, CA: Academic Press; 1994.

Marmottant P, Van der Meer S, Emmer M, Versluis M, de Jong Nico, Hilgenfeldt S, Lohse D. A model for large amplitude oscillations of coated bubbles accounting for buckling and rupture. J Acoust Soc Am. 2005; 118(6):3499–3505.

Patil AV, Rychak JJ, Allen JS, Klibanov AL, Hossack JA. Dual frequency method for simultaneous translation and real-time imaging of ultrasound contrast agents within large blood vessels. Ultrasound Med Biol. 2009 Dec; 35(12):2021–2030. [PubMed: 19828229]

Patil AV, Rychak JJ, Klibanov AL, Hossack JA. Real-time technique for improving molecular imaging and guiding drug delivery in large blood vessels: in vitro and ex vivo results. Mol Imaging. 2011 Aug; 10(4):238–247. [PubMed: 21521555]

Phillips LC, Klibanov AL, Bowles DK, Ragosta M, Hossack JA, Wamhoff BR. Focused in vivo delivery of plasmid DNA to the porcine vascular wall via intravascular ultrasound destruction of microbubbles. J Vasc Res. 2010; 47(3):270–274. [PubMed: 19923850]

Pislaru SV, Harbuzariu A, Gulati R, Witt T, Sandhu NP, Simari RD, Sandhu GS. Magnetically targeted endothelial cell localization in stented vessels. J Am Coll Cardiol. 2006 Nov 7; 48(9): 1839–45. [PubMed: 17084259]

Plesset MS. Dynamics of cavitation bubbles. J Applied Mechanics. 1948; 16:228–231.

Qin S, Caskey CF, Ferrara KW. Ultrasound contrast microbubbles in imaging and therapy: physical principles and engineering. Phys Med Biol. 2009; 54:R27–R57. [PubMed: 19229096]

Rasband, WS. ImageJ. U. S. National Institutes of Health; Bethesda, Maryland, USA: 1997–2011. http://imagej.nih.gov/ij/

Rychak JJ, Klibanov AL, Hossack JA. Acoustic radiation force enhances targeted delivery of ultrasound contrast microbubbles: in vitro verification. IEEE Trans Ultrason Ferroelectr Freq Control. 2005 Mar; 52(3):421–433. [PubMed: 15857050]

Toma C, Fisher A, Wang J, Chen X, Grata M, Leeman J, Winston B, Kaya M, Fu H, Lavery L, Fischer D, Wagner WR, Villanueva FS. Vascular endoluminal delivery of mesenchymal stem cells using acoustic radiation force. Tissue Eng Part A. 2011 May; 17(9–10):1457–64. [PubMed: 21247343]

Unger EC, Matsunaga TO, McCreery T, Schumann P, Sweitzer R, Quigley R. Therapeutic applications of microbubbles. Eur J Radiol. 2002 May; 42(2):160–8. [PubMed: 11976013]

Villanueva FS. Molecular imaging of cardiovascular disease using ultrasound. J Nucl Cardiol. 2008 Jul-Aug;15(4):576–86. [PubMed: 18674725]

Watanabe T, Kukita Y. Translational and radial motions of a bubble in an acoustic standing wave field. Phys Fluids A. 1993 Nov; 11(5):2682–2688.

Yue WM, Liu W, Bi YW, He XP, Sun WY, Pang XY, Gu XH, Wang XP. Mesenchymal stem cells differentiate into an endothelial phenotype, reduce neointimal formation, and enhance endothelial function in a rat vein grafting model. Stem Cells Dev. 2008 Aug; 17(4):785–93. [PubMed: 18522495]

Zhao S, Borden M, Bloch SH, Kruse D, Ferrara KW, Dayton PA. Radiation-force assisted targeting facilitates ultrasonic molecular imaging. Mol Imaging. 2004 Jul; 3(3):135–48. [PubMed: 15530249]

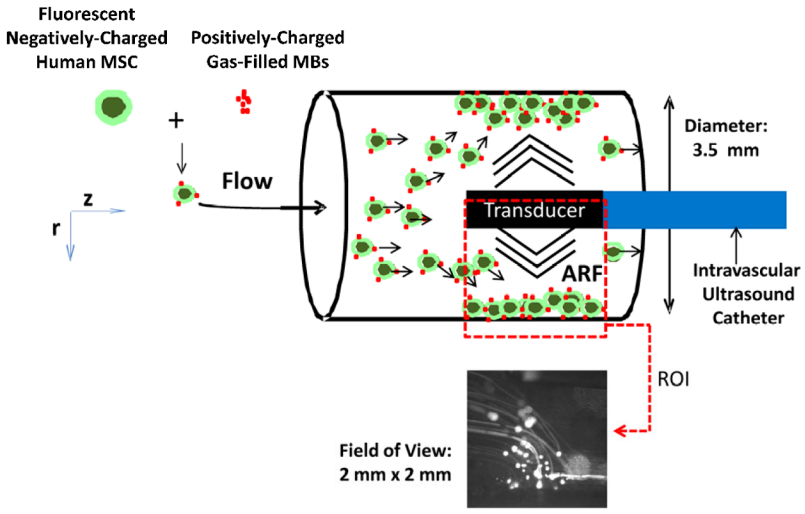

Figure 1.

Experimental setup using a vessel phantom. The negatively charged fluorescent MSCs were labeled with cationic microbubbles. Application of acoustic radiation force caused marginalization and adhesion of the cells to the vessel wall. The region of interest (2 mm × 2 mm) included the lower half portion of the phantom.

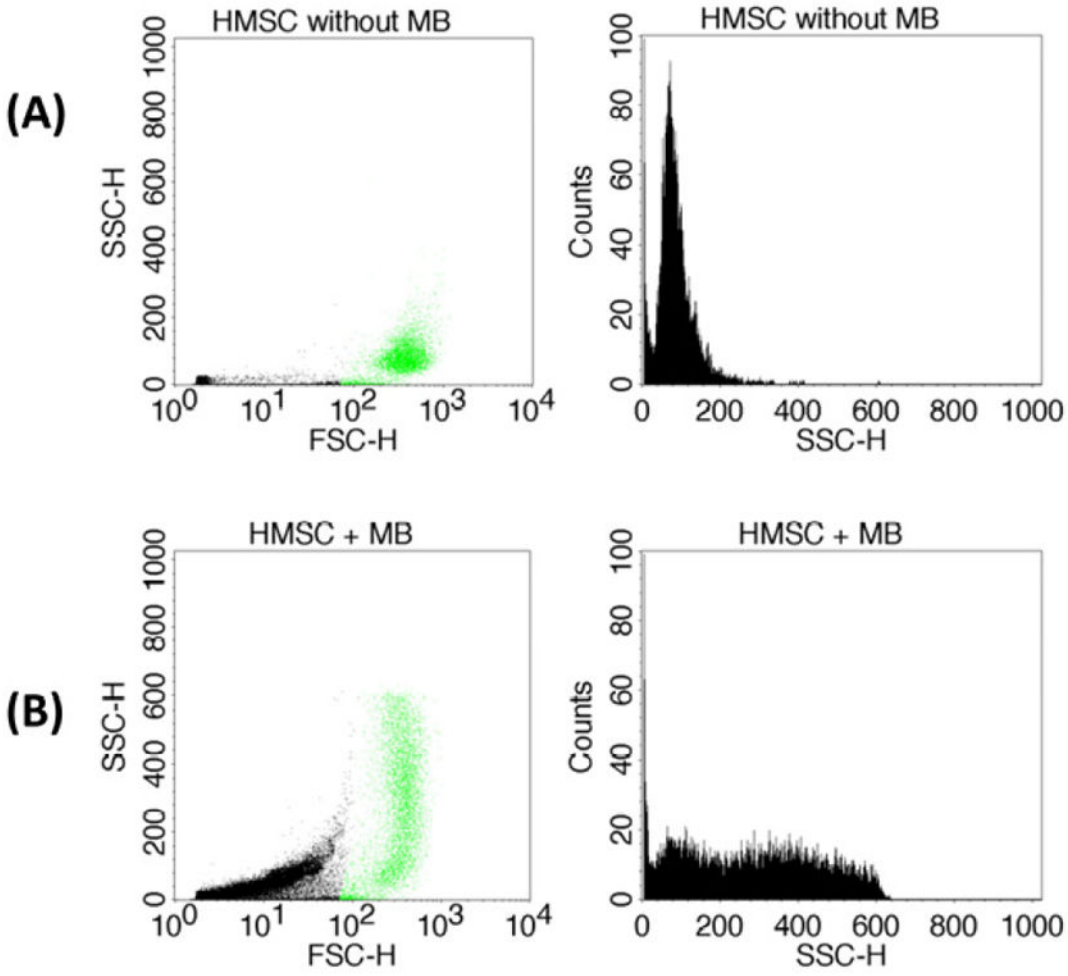

Figure 2.

Quantification of microbubble attachment of MSCs using flow cytometry. (A) Front scatter cross-section (FSC) and side scatter cross-section (SSC) profile (left column) and the distribution of SSC (right column) of fluorescently labeled HMSC alone. (B) FSC/SSC profile (left column) and the distribution of SSC (right column) of fluorescently labeled HMSC, after mixing with cationic microbubbles (1:40 HMSC to MB ratio). In the FSC/SSC profile plots, the fluorescent events of HMSCs were shown in green, while the microbubbles were shown in black. HMSC association with the cationic microbubbles led to increased SSC of the cells relative to HMSCs alone.

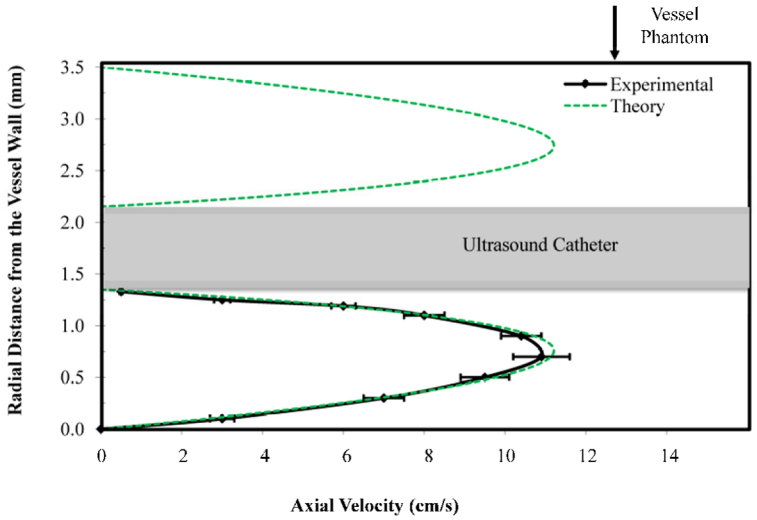

Figure 3.

The axial velocities within the phantom vessel followed a concentric flow pattern (shear stress at vessel wall 1.1 Pa). The experimental data for axial velocities (solid line) with no ultrasound exposure were well correlated with theoretical values (green dashed line).

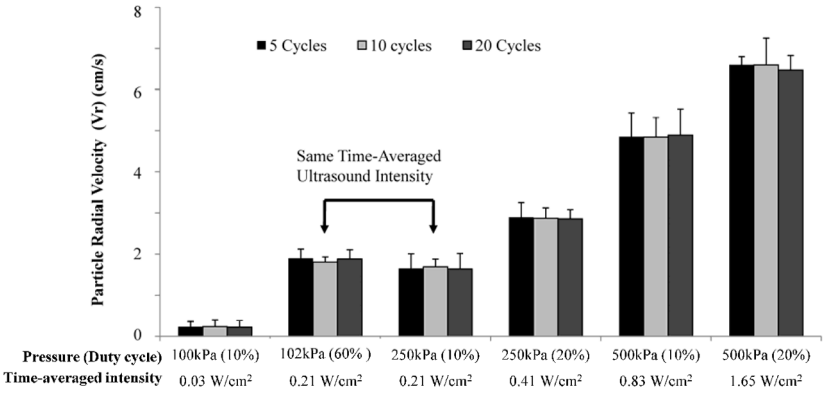

Figure 4.

Radial velocities of MB-cell complexes towards the vessel wall. Bars grouped together had different tone burst configurations but had the same duty cycle and therefore same time-averaged ultrasound intensity.

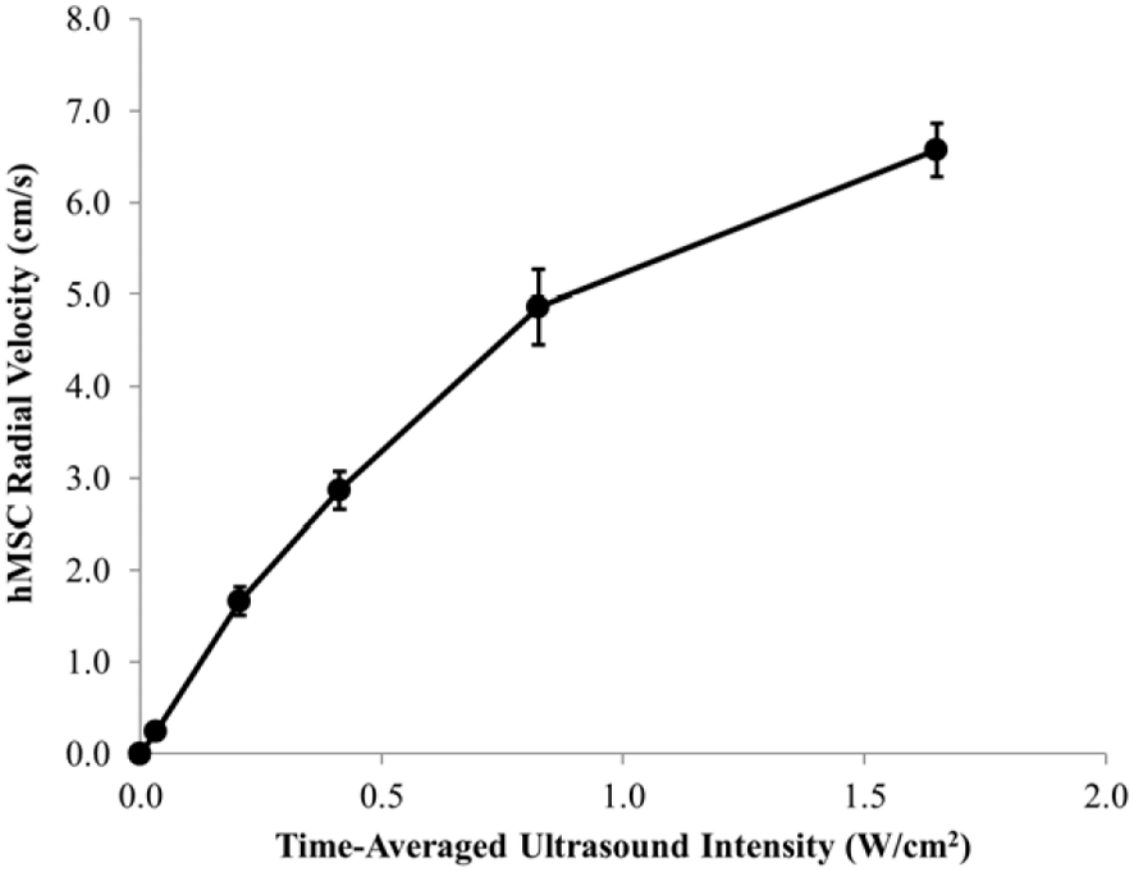

Figure 5.
Experimental radial velocity of the MSCs plotted against time-averaged ultrasound intensity.

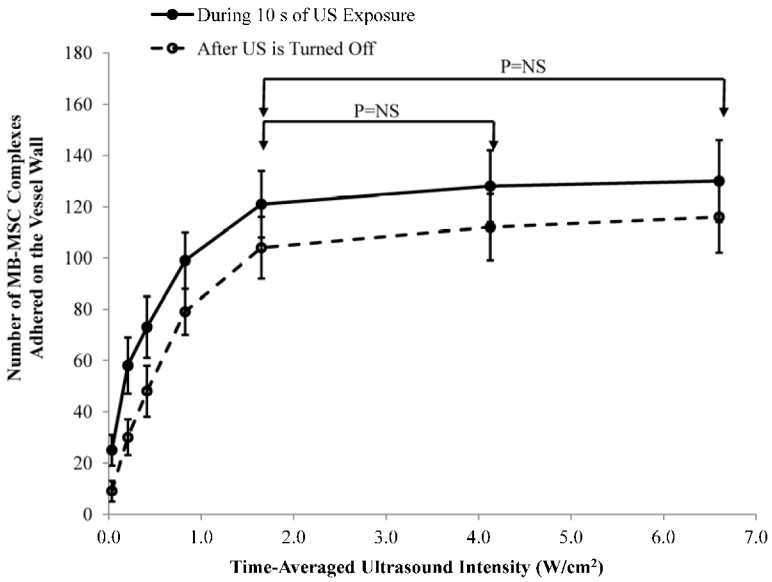

Figure 6.

The total number of MB-MSCs adhered on the vessel wall during 10 seconds of ultrasound exposure (solid line) and 5 seconds after the ultrasound was turned off following the US treatment (dotted line).

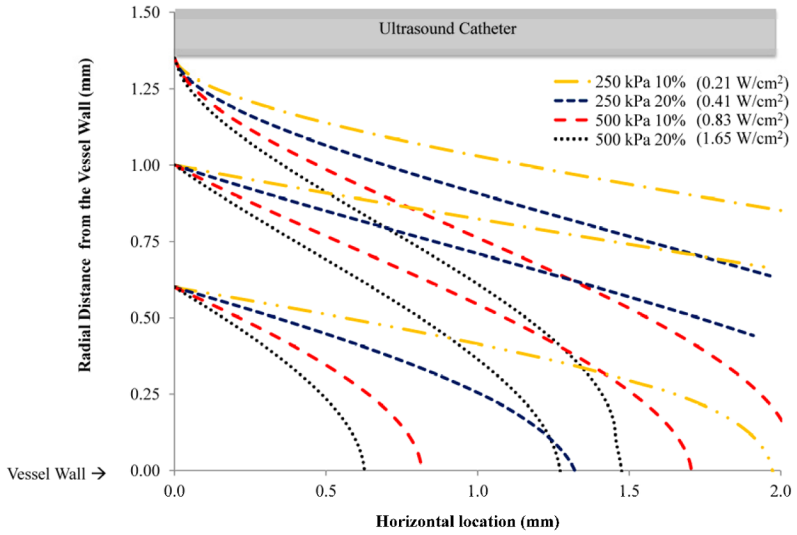

Figure 7.

Flow trajectories of the MB-cell complexes using the measured radial velocity at various ultrasound parameter combinations (axial velocity obtained from the theoretical concentric flow pattern). For simplicity, only MB-cell complexes entering the field of view at 3 different locations (1.35 mm, 1 mm, and 0.6 mm away from the vessel wall) were plotted.

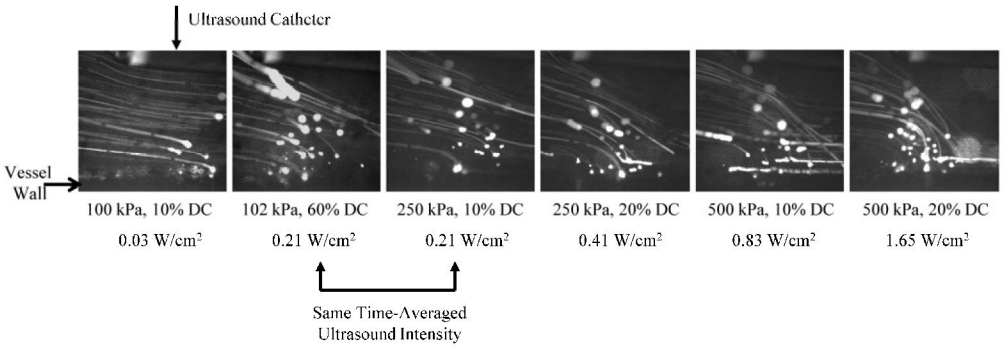

Figure 8.
Flow trajectories of MB-cell complexes for various acoustic pressures and duty cycles after maximum intensity persistence was applied to the recorded images.

Table 1

Details of the ultrasound wave form configuration. Thee Duty Cycles were used (10%, 20% and 60%), each was in turn obtained with 3 different combinations of pulse length (5, 10, 20 cycles) and corresponding pulse intervals.

	10% Duty Cycle			**20% Duty Cycle**			**60% Duty Cycle**		
Pulse Length	5 Cycles	10 Cycles	20 Cycles	5 Cycles	10 Cycles	20 Cycles	5 Cycles	10 Cycles	20 Cycles
Pulse Interval	28 μs	56 μs	112 μs	14 μs	28 μs	56 μs	4.6 μs	9.3 μs	18.6 μs